Monolayer incorporation of nitrogen at Si–SiO_2 interfaces: Interface characterization and electrical properties

Gerald Lucovsky
Departments of Physics, Materials Science and Engineering, and Electrical and Computer Engineering, North Carolina State University, Raleigh, North Carolina 27695-8202

(Received 29 May 1997; accepted 15 September 1997)

This article presents a low-temperature plasma-assisted approach for the preparation of Si–SiO_2 interfaces with monolayer concentrations of bonded nitrogen atoms (N atoms) at that interface. Localization of N atoms at Si–SiO_2 interfaces has been established by on-line Auger electron spectroscopy (AES), off-line secondary ion mass spectrometry, and optical second harmonic generation. On-line AES studies have established that excess suboxide bonding in interfacial transition regions occurs during plasma-assisted oxidation using N_2O and O_2 source gases, and that a postoxidation rapid thermal anneal at 900 °C for 30 s in an inert ambient reduces the concentration of these suboxide bonding groups. Defect generation at plasma nitrided interfaces in field effect transistor devices is reduced compared to similar devices in which Si–SiO_2 interfaces are formed by furnace oxidation in O_2. © *1998 American Vacuum Society.* [S0734-2101(98)02101-0]

I. INTRODUCTION

Monolayer concentrations of N atoms have been incorporated at Si–SiO_2 interfaces by several different techniques including (i) conventional furnace oxidation in N_2O (Ref. 1), (ii) rapid thermal oxidation in N_2O and NO (Refs. 2 and 3), (iii) nitridation, or oxynitridation processes following oxidation or oxide deposition, and (iv) remote plasma assisted oxidation and chemical vapor deposition.[4,5] The first three processes are performed at high temperatures, $>1000\,°C$, whereas the plasma-assisted process of this article incorporates comparable N-atom concentrations at a substrate temperature of 300 °C. However, the plasma-assisted approach requires a low-thermal budget rapid thermal anneal (RTA), e.g., for 30 s at 900 °C (or an *equivalent* thermal exposure) to provide improved electrical reliability with respect to devices with thermally grown interfaces.[5] The RTA accomplishes several things: (i) it reduces the concentration of excess suboxide bonding groups at the Si–SiO_2 interface,[6] and (ii) provides structural relaxation of local bonding in the SiO_2 dielectric layer; e.g., promoting increases in the bonding stretching frequency of the Si–O–Si group, which in turn are related to increases in the average value of the Si–O–Si bond angle.[7] This article focuses on interface nitridation by the low-temperature plasma-assisted process, addressing several aspects of the N-atom incorporation: (i) preferential bonding of N-atoms at Si–SiO_2 interfaces; (ii) relaxation of excess interfacial suboxide bonding by the postoxidation/deposition RTA, and (iii) electrical performance of devices with nitrided interfaces. The article explains significant differences between N-atom incorporation by furnace oxidation/nitridation and plasma processing that derive from the availability of charged and metastable species in the plasma processing. Section II discusses experimental aspects of the plasma-assisted processing, including the use of on-line Auger electron spectroscopy (AES) to track two aspects of the bonding chemistry at the Si–SiO_2 interface: (i) N-atom incorporation, and (ii) reduction of suboxide bonding by the 900 °C RTA. Section III discusses preferential bonding of N atoms at Si–SiO_2 interfaces. Section IV includes results of *ex situ* interface characterization including optical second harmonic generation (SHG),[8–10] that provide additional support for (i) interfacial nitrogen atom incorporation, and (ii) interface relaxation after the RTA. Section V discusses the results of electrical measurements made on devices with nitrided Si–SiO_2 interfaces, and Sec. VI summarizes the results of this study.

II. EXPERIMENTAL RESULTS

A. Interface processing and AES characterization

In previous publications,[4,5,11] a two step process for the formation of thin gate dielectrics with nitrided interfaces has been discussed. These studies have demonstrated that monolayer concentrations of N atoms at Si–SiO_2 interfaces improve reliability in field effect transistors (FETs) with ultrathin gate dielectrics (<6 nm thick) with respect to FETs with gate oxide dielectrics formed by conventional furnace oxidation. In particular, interfacial nitridation improves device lifetimes by decreasing defect generation by hot electrons.[5] The 300 °C plasma processing is performed in two separate steps: (i) a 30 s plasma-assisted oxidation using charged and neutral molecular species transported out of a remotely excited He/N_2O plasma that promotes N-atom incorporation at the Si–SiO_2 interfaces and additionally forms $\sim$0.5–0.6 nm of oxide layer over that interface, and (ii) a 300 °C plasma assisted film deposition process in which using (a) charged and (b) neutral metastable molecular species transported out of a remotely excited He/N_2O plasma and reacted with downstream injected SiH_4 to promote the formation of the remainder of SiO_2 dielectric.[11] Even though the overlayer dielectric is prepared from a N_2O source gas, secondary ion mass spectrometry (SIMS) measurements have established that this plasma deposited layer is a stoichiometric oxide,

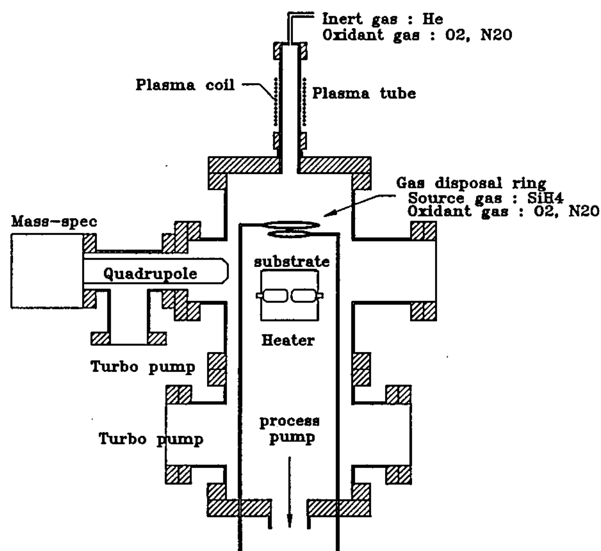

FIG. 1. Schematic drawing of remote plasma processing chamber.

rather than an oxynitride alloy. This article concentrates on the initial oxidation step, comparing oxidation in remotely excited He/N_2O, He/O_2, and sequential He/N_2O and He/O_2 plasmas. The RF plasmas were excited at 13.56 MHz at a power level in the range of 15–30 W. Chemical and structural relaxation of the interface necessary for achieving device level performance and reliability take place during a 30 s RTA in an inert ambient (e.g., Ar) or an equivalent thermal exposure during downstream processing (e.g., during dopant activation of polycrystalline Si gate electrodes and/or source and drain junctions). The initial plasma-assisted oxidation/nitridation step is performed on a wet chemistry prepared H-atom terminated surface, and has been shown to (i) yield monolayer N-atom concentrations at the Si–SiO_2 interface,[4] and (ii) produce approximately 0.5–0.6 nm of SiO_2 onto which the remainder of the oxide film is deposited by the remote plasma chemical-vapor deposition step.[11] Most importantly, as pointed out in Ref. 11, the two-step plasma processing approach provides separate and independent control of the chemical bonding at interface in the oxide film through the formation of the thin oxide layer.

Experimental studies have been performed in a multichamber UHV-compatible processing/analysis system which provides fixtures for the plasma processing steps, as well as on-line AES. Figure 1 indicates a schematic representation of the plasma processing chamber. The plasma generation tube has a diameter of approximately 25.4 mm, the chamber diameter is 200 mm, and the nominal distance from the center of the plasma coil to the substrate is 300 mm. The gas dispersal rings are positioned approximately halfway between the end of the plasma tube and the deposition substrate. In addition, one of the processing chambers also includes provisions for performing real-time process characterization by mass spectroscopy (MS) and optical emission spectroscopy (OES). Figures 2 and 3 present the results of on-line AES measurements in the Si_{LVV} spectral range for interrupted plasma assisted predeposition oxidation/nitridation. The process gas mixtures in Figs. 2(a), 2(b), and 3 are He/O_2 and He/N_2O, respectively. In all cases, the plasma power at 13.56 MHz was 30 W.

Consider first Figs. 2(a) and 2(b); three features in the AES spectra that yield information relative to interface bonding are the (i) Si–Si feature at $\sim 92 \pm 1$ eV, (ii) Si–N feature at 83 ± 1 eV, and (iii) Si–O feature at 76 ± 1 eV. As shown in Fig. 3, the 83 eV Si–N feature correlates with the presence of a N_{KLL} spectral feature at ~ 380 eV. There are additional contributions to the Si_{LVV} region spectra from suboxide, SiO_x, or transition region bonding arrangements that are present at as-grown Si–SiO_2 interfaces and also occur at about 80–85 eV.[6] These can be differentiated from Si–N bonding by the occurrence of the N_{KLL} spectral AES feature as discussed above. These comparisons are qualitative in nature, and no attempts have been made to quantify them, as for example by subtractive procedures. In addition, the effects of the 900 °C RTA, which are discussed in detail later on in this section, will help to clarify some of the spectroscopic issues relative to the SiO_x and SiN contributions to the 83 eV AES feature.

Following the results in Ref. 11, the thickness of the oxide is determined from the relative amplitudes of the Si–Si signal at 92 eV which comes from the Si substrate, and the Si–O feature at 76 eV which comes from the oxide bonding. This process uses published data for the escape depth of the AES electrons in the Si_{LVV} region. The results obtained for oxide thickness (t_{ox}) as a function of time can then be fit to a power law function, $t_{ox} = A(t)^b$, where $A = 0.71 \pm 0.02$ nm, and $b = 0.28 \pm 0.01$; and t is the time in minutes.[12] This functional form is valid for the range of oxide thicknesses explored by the plasma-assisted oxidation process for which $t_{ox} < 2.5$ nm. Moreover, the function form does not represent an attempt to fit to a particular model or theory of oxidation, but rather is used to emphasize two points: (i) the initial oxidation rate is very rapid, and (ii) the oxidation rate drops off dramatically with increasing time, so that using a linear–linear plot, the data would appear to represent a saturation of the oxide growth process. The spectrum taken at 15 s is for an oxide layer that is 0.48 ± 0.02 nm thick, and displays features from the Si substrate, (the Si–Si bond), and from the interface and/or the thin oxide layer (the Si–N and Si–O features). In addition, O_{KLL} and N_{KLL} features are also evident at higher AES electron energies (see Fig. 3). As the oxidation process is continued, the Si–Si and Si–N Si_{LVV} features diminish in strength relative to the Si–O feature at 76 eV which grows with increasing oxide thickness. The decreased strength of the N-related Si_{LVV} signal also correlates with the disappearance of the N_{KLL} feature at higher eV. The combination of these AES results demonstrates that (i) N atoms are incorporated at, or in the immediate vicinity (< 0.5 nm) of the Si–SiO_2 interface, and (ii) they are not incorporated in the bulk of the oxide film. The incorporation of N atoms at monolayer concentration levels following plasma-assisted oxidation in the He/N_2O source gas mixture has been confirmed by SIMS.[4,5]

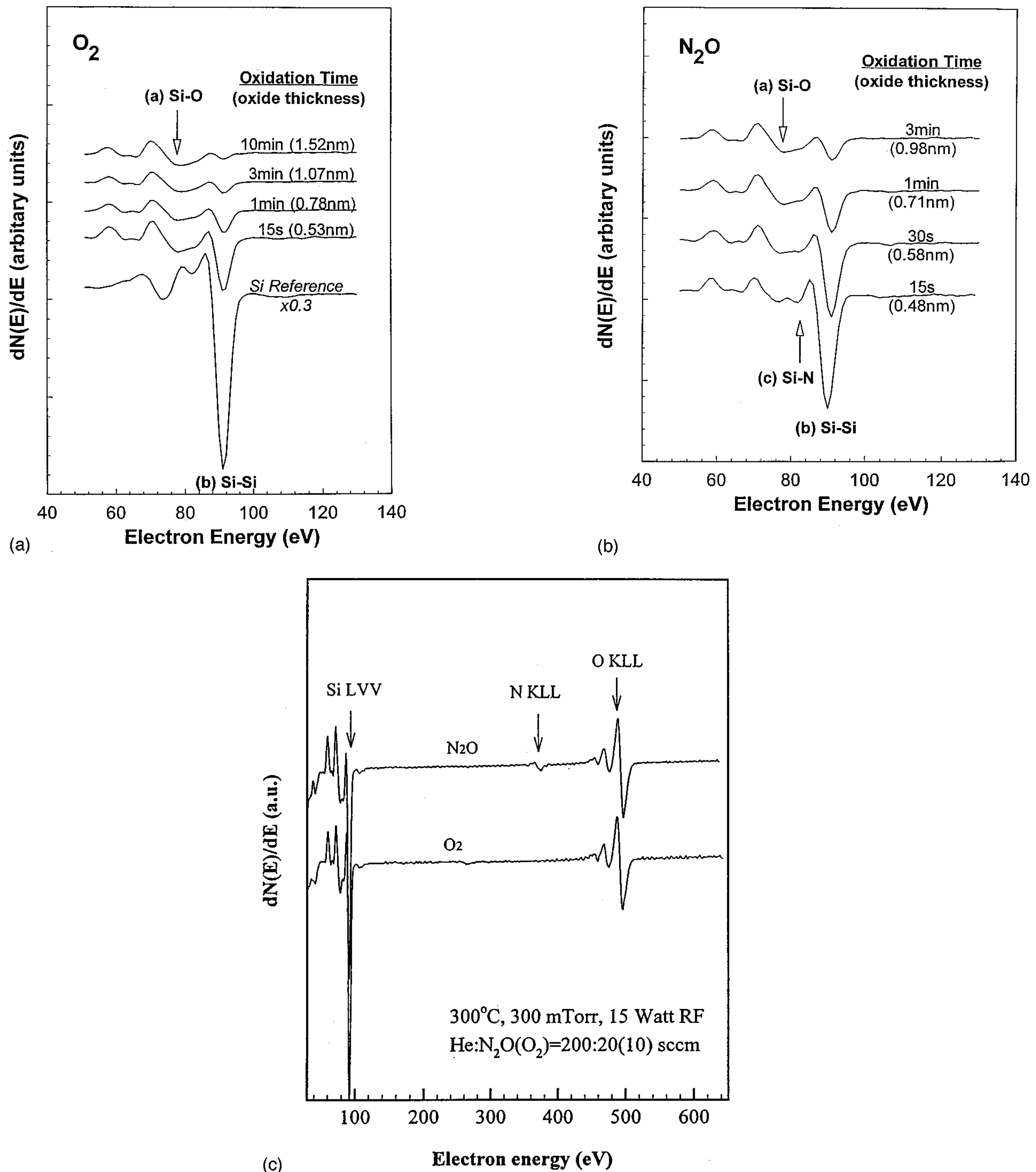

FIG. 2. AES spectra in the Si_{LVV} region for plasma-assisted oxidation in (a) O_2 and (b) N_2O.

Finally, optimum processing conditions for device quality interfaces, as monitored in metal-oxide-semiconductor (MOS) capacitors and FETs, are a 15 s predeposition process using O_2, and a 30 s process using N_2O.[4]

Figures 4(a) and 4(b) indicate derivative Si_{LVV} AES spectra for oxide layers grown in (a) He/O_2 and (b) in He/N_2O, respectively, that are approximately 0.5 nm thick (i) as grown at 300 °C and (ii) after a 30 s 900 °C RTA.[6] From the traces shown in Fig. 4, we observe that the relative amplitude ratio, $\{I(83\text{ eV})/I(76\text{ eV})\}_{\text{after RTA}}/\{I(83\text{ eV})/I(76\text{ eV})\}_{\text{as grown}}$, decreases after the anneal (see Table I). The feature at ~76 eV is due to SiO_2-like bonding; i.e., Si atoms with four O-atom neighbors, while the feature at ~83 eV includes contributions from both suboxide bonding groups; i.e., Si atoms with fewer than four O-atom neighbors, as well as Si–N. The suboxide contribution is identified from studies of Si surfaces that have been exposed to quan-

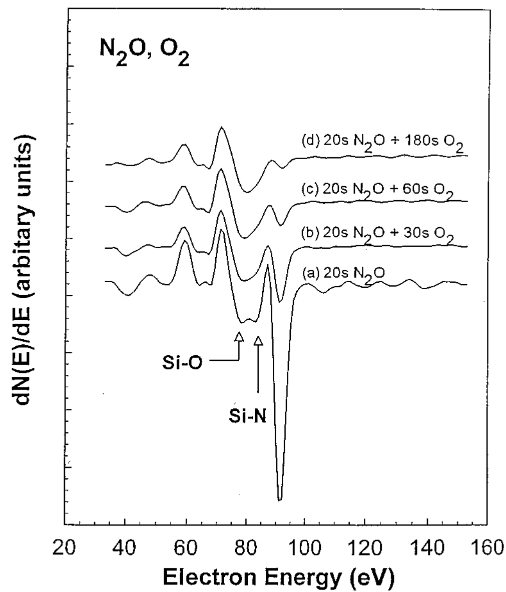

FIG. 3. AES spectra including the Si_{LVV}, N_{KLL} and O_{KLL} features for the plasma-assisted oxidation in O_2 and N_2O.

tities of oxygen insufficient to provide for complete oxide surface coverage [see Fig. 2(a)], whereas the Si–N contribution has been identified through studies of bulk Si_3N_4. Figures 5(a) and 5(b) indicate similar spectra for films grown by RTO in O_2 and N_2O at 800 °C, and after a 30 s 900 °C RTA. Smaller decreases in the amplitude ratio occur for these samples. To confirm that changes in the amplitude ratios in Figs. 4 and 5 were not due to oxidation during the RTA, the relative amplitudes of the Si–Si Si_{LVV} feature at ~92 eV, and the O_{KLL} feature at ~510 eV were also monitored and found to be the same before and after the RTA. Analysis of results displayed in Figs. 4(a), 4(b), 5(a), and 5(b) is the basis for values of $\{I(83\text{ eV})/I(76\text{ eV})\}$after RTA/$\{I(83\text{ eV})/I(76\text{ eV})\}$as grown presented in Table I. Since each of these ratios is less than one, this means that there is a relative decrease in the amplitude of the 83 eV feature after the anneal. It is important to recognize that a perfectly flat interface with a superficial SiO_2 layer would display three types of bonding as studied by AES (i) Si–Si bonding from the substrate, (ii) SiO_2 bonding the bulk oxide; and (iii) SiO_x bonding from the interfacial boundary between the Si and SiO_2 (the particular SiO_x bonding is determined by the Si surface). The differences between the AES spectra in Figs. 4 and 5, as grown and after the RTA reflect the reduction of excess suboxide bonding above what must occur at a perfectly flat, idealized interfacial boundary between Si and SiO_2. Based on the AES studies reported in this article, we have not been able to differentiate between the different SiO_x bonding arrangements. Even though the differences the AES spectra before and after the RTA in Figs. 4 and 5 are small, they are reproducible, and always in the same direction with regard to the relative magnitudes of the two features under consideration. This gives us confidence that these measurements are significant.

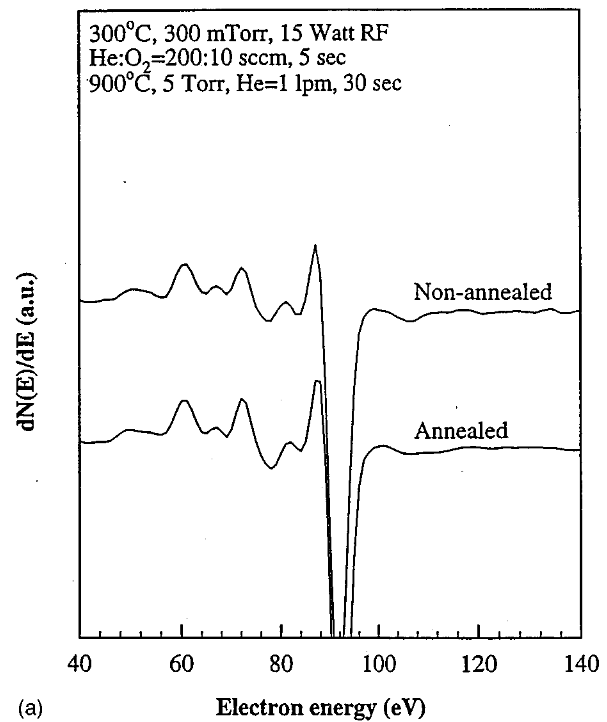

(a)

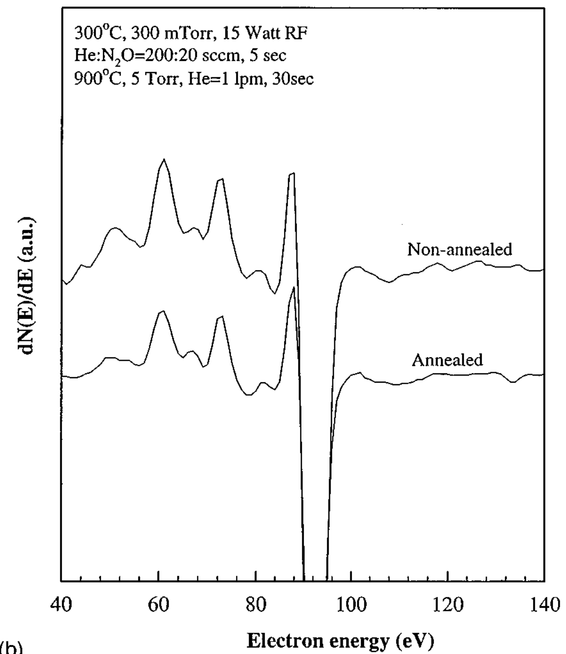

(b)

FIG. 4. Derivative Si_{LVV} AES spectra for oxide layers grown in (a) He/O_2 and (b) in He/N_2O, respectively, by RPAO that are approximately 0.5 nm thick as grown at 300 °C and after a 30 s 900 °C RTA.

In addition, we have prepared samples with oxides that are ~1.0 nm thick by the plasma-assisted oxidation process, and these have been studied by x-ray photoelectron spectroscopy (XPS). Reductions in suboxide bonding are clearly evident in the raw data, between the as-deposited and annealed samples given further support to the changes seen in the AES spectra for similarly prepared interfaces.

TABLE I. Changes in the relative intensities of the SiO_x and SiO_2 AES at approximately 83 and 76 eV, respectively.

Interface formation	{I(83 eV)/I(76 eV)}after RTA / {I(83 eV)/I(76 eV)}as grown
Plasma O_2	0.88±0.02
Plasma N_2O[a]	0.79±0.02
RTO O_2	0.80±0.02
RTO N_2O[b]	0.86±0.02

[a]Monolayer N-atom bonding at the Si–SiO_2 interface.
[b]No AES detectable interfacial N-atom bonding at the SiO_2 interface.

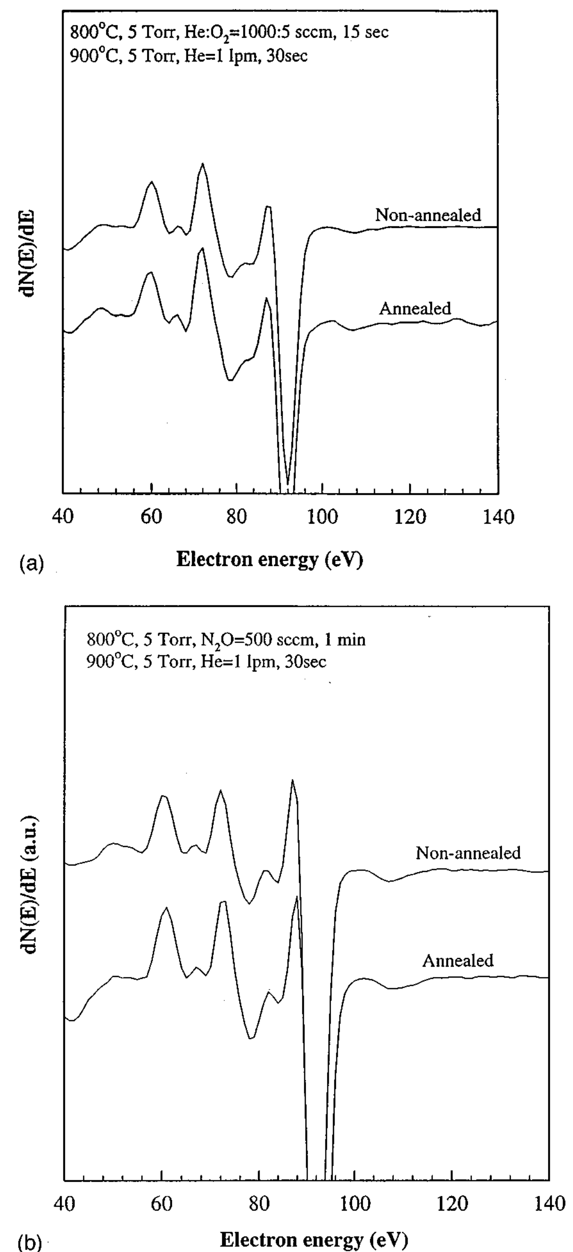

FIG. 5. Derivative Si_{LVV} AES spectra for oxide layers grown in (a) He/O_2 and (b) in He/N_2O, respectively, by RTO that are approximately 0.5 nm thick as grown at 300 °C and after a 30 s 900 °C RTA.

B. *In situ* studies of plasma processing

Figures 6(a)–6(c) display results of *in situ* MS and OES measurements of the excited and neutral molecular species that are present during plasma assisted oxidations using the He/N_2O and Ar/N_2O source gas mixture. The MS probe is positioned near the deposition substrate, and the OES data are taken from the plasma generation region. Consider first the MS data in Fig. 6(a) for He/N_2O; these data demonstrate that the dominant, and essentially the only charged species available in high concentrations for the levels low plasma power (~30 W) used in these studies is NO^+. The MS measurements were done with ionizer off. The OES data in Figs. 6(b) and 6(c), respectively, are for remote plasma excited He/N_2O and Ar/N_2O mixtures and demonstrate significant concentrations of the neutral excited nitrogen molecule (N_2^*) and positively charged oxygen molecular ion (O_2^+) are present in the plasma generation region. The N_2^* species is **AAA**. The combination of the OES date in Fig. 6(c) and the MS data in Fig. 6(a) demonstrate that even though O_2^+ ions are generated, they are not transported into the plasma processing part of the chamber for plasma powers $\leqslant$30 W. Finally, the long-lived metastable molecular species O_2^* has been shown to be active in film deposition of SiO_2 thin films by remote plasma CVD, and we propose below that it is also the active species for surface oxidation.[13]

Since the plasma-generated species determine the reaction pathways for interface nitridation, it is useful to discuss some bonding properties of the NO^+ and O_2^* that derive from their respective molecular structures. NO^+ contains ten electrons which accounts for its relatively high stability. It is isoelectronic with N_2 with a comparable binding energy that is characteristic of a bond order of three; i.e., a triple bond, >10 eV.[14] O_2^* has a bond order of two with two electrons in antibonding orbitals. In neutral O_2 molecule two electrons reside in different antibonding orbitals, whereas in O_2^* they reside in the same antibonding orbital. The relative stability of O_2^*, as well as particular aspects of chemical reactivity derive from this aspect of the its electronic structure.

III. NITROGEN BONDING AT Si–SiO_2 INTERFACES

The experimental results presented above have demonstrated that when O- and N-atom active precursor species are both present in a plasma-assisted oxidation process [see Figs. 2(b) and 2(c)] (e.g., N_2^*, O_2^*, and NO^+) N atoms are retained at Si–SiO_2 interfaces in preference to O atoms. Three factors play significant roles in determining which type of interface bonding dominates, Si–O or Si–N: (i) the bond energy; (ii) the mechanical strain; and (iii) the chemical strain. Using nominal bond energies from Ref. 14, the Si–O bond energy of 3.8 eV is greater than the Si–N bond energy of 3.5 eV, so that based on bond energy alone N-atom terminated interfaces are not expected. However, two different strain energy contributions combine to favor N-atom interfacial bonding. Experiments performed in our laboratory and elsewhere,[15,16] have established that the mechanical strain energy is large (~5×10^9 dynes cm^{-2}) and compressive in the SiO_2 layer, and large and tensile in the Si substrate at Si–SiO_2 inter-

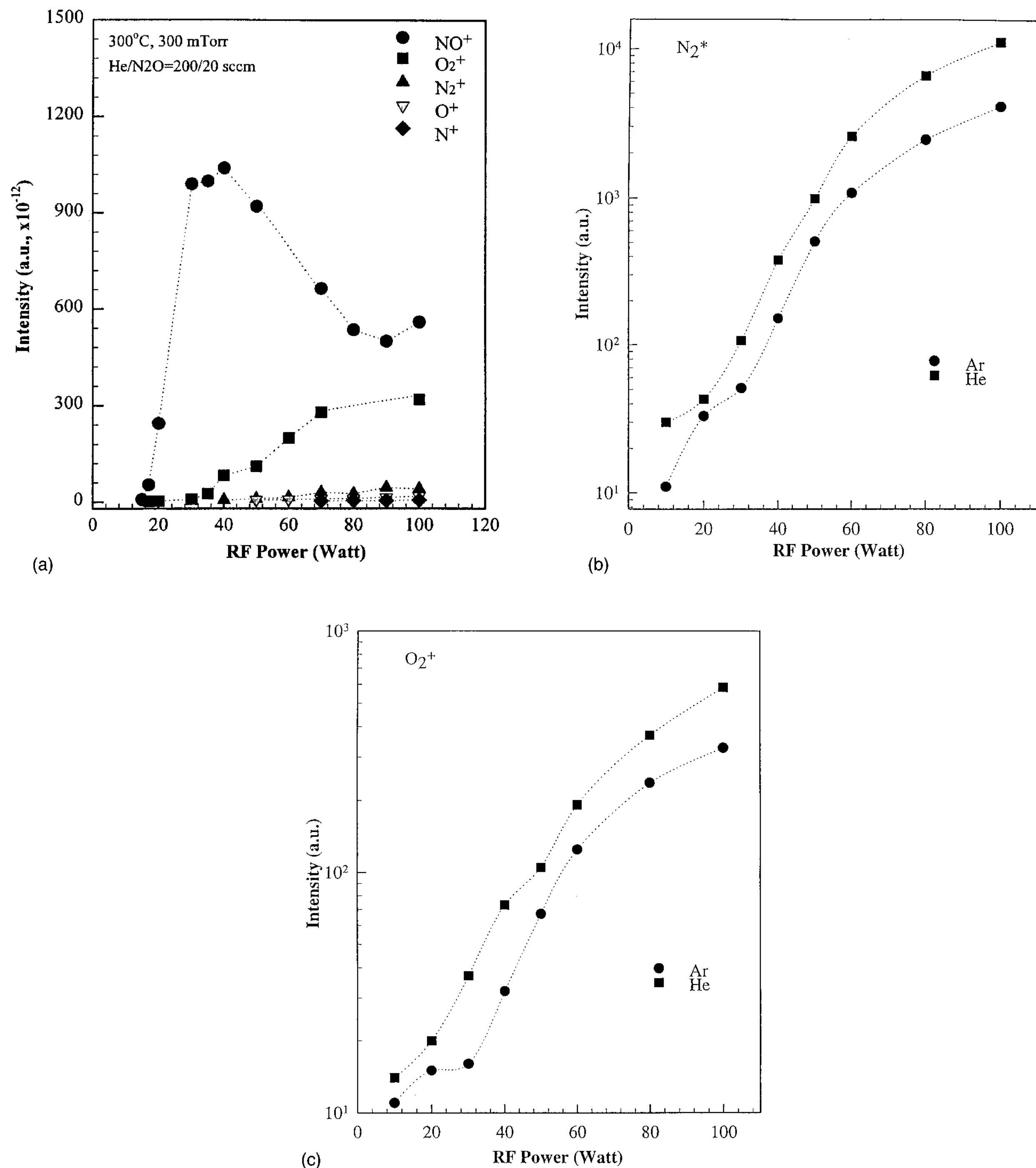

FIG. 6. (a) Relative intensity of mass spectrometry signal for NO^+ as a function of rf plasma power. OES signals for (b) N_2^* and (c) $O_2{}^+$ for plasma excitation of N_2O/Ar and N_2O/He mixtures.

faces, while the mechanical strain energy is tensile or weakly compressive in Si_3N_4 layers on Si substrates. The chemical strain energy of Si–Si bonds at the chemical interface and defined changes in these Si–Si bond energies due to charge withdrawal is determined by the extent of charge exchange at the interface. The electronegativities as measured on the Pauling scale of $X_{Si}=1.9$; $X_N=3.0$, and $X_O=3.5$, (Ref. 14) indicate that less charge withdrawal is expected to occur from the Si substrate with Si–N interface terminations, than with Si–O terminations. This means that the mechanical and chemical strain energies are large and additive for interfacial Si–O bonds, whereas for interfacial Si–N bonds they are significantly smaller, with the mechanical and chemical strains being possibly subtractive. Since the total binding energy equals the bond energy plus the sum of the strain energies, Si–N bonding is favored if the difference between the sums of these two strain energies terms is greater than about 0.3 eV. Since N interfacial bonding occurs for both plasma

and thermal processing, this appears to be the case. Additional experimental, theoretical, and/or model studies are necessary to pin this point down and determine which strain effect dominates, the chemical or the mechanical. In addition, it is possible for the threefold coordinated N atoms to make two bonds with Si atoms and the third bond with a Si atom of the oxide, whereas, interfacial O atoms must in effect bridge the Si substrate and the overlying oxide by making one Si–O bond to Si substrate and one to the oxide. Finally, the incorporation of interfacial N atoms may be determined by kinetics rather than equilibrium considerations of the different contributions to the binding energy noted above.

IV. INTERFACE CHARACTERIZATION BY OPTICAL SHG

The new results presented in Sec. II B for reduction of excess suboxide bonding by the 900 °C RTA help to explain some previously published optical SHG data.[8–10] These data are summarized below, where Table III includes the results of optical SHG studies on vicinal Si(111) off cut in the 112-bar direction. The interface processing conditions are indicated in the table, and include the optimum plasma-assisted oxidation/nitridation processes discussed above. The values of the phase difference ($\Delta\Phi$) and the amplitude ratio (A_1/A_3) are obtained from a harmonic analysis of the azimuthal dependence of a normalized SHG response taken at a 45 degree angle of incidence using a Nd:YLF (1.17 eV) laser source. The azimuthal angle, Ψ, is measured from the 112-bar direction. The $A_1\cos(\Psi)$ term reflects a symmetry axis perpendicular to the step direction (i.e., 112 bar), and the $A_3\cos(3\Psi)$ term reflects the bonding symmetry of the Si atoms on (111) surface. $\Delta\Phi$ is a phase difference determined by different chemically specific resonance energies at the step and terrace atom bonding sites. The electric field (E_2) at the second harmonic frequency (photon energy=2.34 eV) is given by[8–10]

$$E_2=[A_1\cos(\Psi)+A_3\cos(3\Psi)\exp(i\Delta\Phi)]. \quad (1)$$

The intensity of the SHG signal is proportional to $(E_2)\times(E_2)^*$. SHG signals with the harmonic components in Eq. (1) come only from the Si–SiO$_2$ interface, and are sensitive to the termination chemistry at that interface.[8,10] An important aspect of the SHG characterization relates to the fact that the phase difference between the two harmonic components of the electric field in Eq. (1) can be determined from a harmonic analysis of the anisotropy data. This is manifestation of the coherent nature of the SHG. Referring to the table: (i) $\Delta\Phi$ and the amplitude ratio are essentially the same for all samples not subjected to the RTA (ii) $\Delta\Phi$ is different for different interface processing for all of the samples subjected to the RTA, and (iii) the amplitude ratio after the RTA is different from samples not subjected to the RTA, but is essentially the same for all processing combinations. Predeposition, plasma oxidation/nitridation times of 15 s for O$_2$ and 30 s for N$_2$O have been shown to be sufficient to yield good device performance when combined with oxide deposition by remote PECVD,[4,11] and a thermal exposure equivalent to the 30 s, 900 °C RTA.[4] Combined with SIMS results in Ref. 4, the AES and optical SHG demonstrates that remote plasma-assisted oxidation in N$_2$O produces an Si–SiO$_2$ interface at which there is approximately one monolayer N atoms between the Si substrate and the oxide. In particular: (i) the AES results in Fig. 2 demonstrate N-atom incorporation within at most an electron escape depth or 0.6 nm of the Si–SiO$_2$ interface; (ii) the SIMS results in Ref. 4 indicate an integrated N-atom concentration of approximately one monolayer; and (iii) the SHG results discussed in Refs. 8–10 and presented in Table II indicate N atoms at the Si–SiO$_2$ interface; i.e., between the Si substrate and the oxide film. Finally, the interfacial Si–O and Si–N bonding arrangements are visible in the SHG after the 900 °C RTA; i.e., after the suboxide layer has been removed by the chemical reactions that take place during the annealing step.[6]

TABLE II. Summary of results from studies of vicinal Si(111) surfaces off-cut ~5 degrees in the 112-bar direction.

(a) Surface treatment[a]—plasma processing	Phase, $\Delta\Phi$[b]	A_1/A_3[b]
O$_2$-15 s-300 °C	68	0.20±0.02
O$_2$-15 s-30 s 900 °C RTA (0.5% O$_2$/Ar)[c]	23	0.35±0.03
N$_2$O-15 s-300 °C	67	0.21±0.02
N$_2$O-15 s-30 s 900 °C RTA (Ar)	11	0.37±0.04
N$_2$O-30 s-300 °C	65	0.17±0.02
N$_2$O-30 s-30 s 900 °C RTA (Ar)[c]	11	0.35±0.03
(b) Surface treatment—thermally grown interfaces		
Furnace oxidation at 850 °C	72	0.19±0.02
Postoxidation anneal (30 s at 950 °C (0.5% O$_2$/Ar)	23	0.33±0.03

[a]Predeposition RPAO step.
[b]See Eq. (1).
[c]Processing conditions for optimum electrical properties (Ref. 2).

From Table II, the relative phase of the as-grown thermal oxide is 72 degrees, and decreases significantly to ~23 degrees after the 900 °C anneal.[13] In a similar way the relative phases for interfaces formed by 300 °C plasma-assisted oxidation also change markedly after a similar 30 s 900 °C RTA. There are no significant differences between Δ_{13} for plasma-assisted oxidation interfaces as formed at 300 °C in N$_2$O and O$_2$, even though SIMS and on-line AES show a nitrogen terminated interface for the N$_2$O process. However, after the RTA, there are significant differences in Δ_{13}. Δ_{13} is equal to 23 degrees for the oxygen terminated interfaces, the same value as obtained after annealing a thermally grown interface, but is reduced to 11 degrees for the nitrogen terminated interface. The SHG results are then consistent with a significant change in interface bonding. Combining the SHG results with the AES results presented above, it is concluded that the Δ_{13} values of 67–72 degrees are characteristic of suboxide bonding arrangements, whereas the smaller values of Δ_{13} of 23 and 11 degrees are indicative, respectively, of more nearly idealized bonding arrangements with O- and N-atom interfacial bonding.

TABLE III. Electrical properties of nitrided interfaces: (a) interface defects in MOS capacitors, (b) initial performance of FETs, and (c) reliability of short channel FETs 5.5 nm gate oxide-0.5 μm channel length.

(a) Interface preparation		Interface traps, D_{it} (10^{10} cm^{-2} eV^{-1})
(a) plasma processed-300 °C		
oxygen terminated		1.0±0.5
nitrogen terminated		1.0±0.5
N–H terminated		20 ±4
N–H anneal→N-terminated (after RTA)		1.0±0.5
(b) thermal oxidation		1.0±0.5
(b) Interface preparation	**Threshold voltage (V)**	**Peak mobility (cm^2 V^{-1} s^{-1})**
Thermal oxidation 900 °C	0.33±0.3	450±5
Plasma oxidation 300 °C+RTA	0.38±0.03	460±5
Plasma nitridation 300 °C+RTA	0.41±0.03	460±5
(c) Interface preparation	**$\Delta g_m/g_m$**	**$\Delta V_t/V_t$**
Thermal oxidation 900 °C	−16.2%	+9.9%
Plasma oxidation 300 °C+RTA	−20.5%	+14%
Plasma nitridation 300 °C+RTA	−12.5%	+6%

V. ELECTRICAL PROPERTIES OF NITRIDED INTERFACES

The electrical properties of MOS capacitors and FETs prepared by remote plasma processing and RTAs have been reported elsewhere.[5,6] In this article we summarize the results of these studies in Table III in order to emphasize the benefits of interfacial N-atom incorporation in reduced performance degradations due to hot carrier injection during device operation. Three types of interface formation processes are compared: (i) O-atom terminated interfaces prepared by plasma-assisted oxidation in O_2, (ii) N atom terminated interfaces prepared by plasma-assisted oxidation in N_2O, and (iii) O atom terminated interfaces prepared by conventional furnace oxidation in O_2. The device structures prepared by furnace oxidation provide a reference point for the effectiveness of the plasma processing RTA approach.

The results in Table III demonstrate that (i) the levels of interface traps, as detected by the analysis of capacitance–voltage ($C-V$) measurements are essentially the same for interfaces prepared in all three ways [note that the plasma processed devices were prepared at 300 °C, and then subjected to a postmetallization anneal (PMA) in N_2/H_2 at 400 °C, whereas the furnace oxidation interface was prepared at 900 °C and subjected a similar PMA], (ii) the maximum values of the electron channel mobilities were independent of the processing, (iii) the threshold voltages for FET operation differed, with the differences between the plasma-processed interfaces and the thermal oxide arising from differences in dopant redistribution between thermal and plasma-assisted oxidation processes, and (iv) the hot carrier stress measurements indicate that the degree of degradation was lowest for decreases in the maximum transconductance and increases in the threshold voltage for the nitrided plasma processed interface. The most note worthy aspect of these comparisons is the increased reliability of the devices with the N terminated interfaces. A chemical bonding model, discussed in Refs. 17 and 18, has been invoked to explain the increased reliability of nitrided interfaces. For example, at an Si–SiO_2 interface that has not been nitrided, hole trapping at O-atom sites can induce the formation of fixed positive charge and interfacial traps by a displaced motion of H atoms from interfacial Si–H bond via the following reaction:

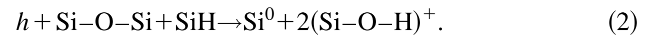

$$h+\text{Si–O–Si}+\text{SiH}\rightarrow\text{Si}^0+2(\text{Si–O–H})^+. \quad (2)$$

The energy barrier after hole trapping on the near-interfacial O-atom is small, <0.1 eV; however because of the threefold coordination of N atoms in a planar bonding arrangement, there is a relatively large barrier, ~ 2 eV, for the creation of the fourfold coordinated, positively charged N-atom defect center.

In addition to what is presented in Table III, it was further observed that the rate of fall-off of channel mobility with the channel surface electrical field was essentially the same for the FETs with (i) plasma process nitrided interfaces and (ii) with interfaces formed by thermal oxidation. The mobility falloff is determined by interface roughness. Consistent with the AES results we have presented, and with other studies of interface roughness by XPS[19] and transmission electron microscopy,[20] the mobility studies on the FETs demonstrate that interface roughness is reduced to the same degree by a post oxidation thermal exposure equivalent to the 900 °C RTA. The development of a transition region with suboxide bonding during the thermal oxidation of silicon had been proposed earlier,[21,22] and is verified by the experiments reported in this article that this occurs for two additional oxidation processes (i) low-temperature plasma-assisted oxidation, and (ii) RTO at 800 °C.

VI. SUMMARY

This article has demonstrated that N atoms can be incorporated at an interface between crystalline Si and an SiO_2 layer by forming the interface and oxide film by a 300 °C remote plasma-assisted nitridation/oxidation process using N_2O as the source gas for both N and O atoms. The article

has proposed reaction pathways for N-atom incorporation and removal from buried Si–SiO_2 interfaces for the remote plasma assisted process. Excess suboxide bonding is a consequence of the oxidation process, and this is reduced after a 30 s, 900 °C RTA or an equivalent thermal exposure at a later stage of the processing. Differences in reaction pathways are expected between plasma and thermal processing due to differences in precursor species, in particular the generation of charged species by the remote plasma processing approach, and the absence of charged precursors and long-lived metastables such as O_2^* for the furnace processes.

Finally, there are three other recently reported studies that have addressed surface roughness/interfacial transition regions and changes that take place on annealing. Gibson *et al.* have used TEM interference techniques and demonstrated significant interfacial smoothing for thermally grown oxides subjected to a 900 °C anneal.[20] Downer and co-workers have used optical SHG to study Si–SiO_2 interfaces formed on Si(100) and have observed irreversible changes in the response from interfaces formed at low temperatures, ~800 °C, that were subsequently subjected to 900 °C thermal exposure.[23] Finally, Matsumura and co-workers showed that ultrathin oxides (~3 nm thick) prepared by thermal oxidation at 650 °C and annealed at 850 °C showed improved performance with respect to stress-induced increases in tunneling currents.[24] They also found that oxides grown at 850 °C showed improved stress resistance after an anneal at 850 °C. These improvements were correlated with reductions in interface roughness as measured by x-ray scattering techniques.

ACKNOWLEDGMENTS

This work is supported by the Office of Naval Research, the National Science Foundation, and the Semiconductor Research Corporation. The author acknowledges the results of research performed by several of (i) his former students and postdoctorals: Y. Ma, D. R. Lee, and T. Yasuda, and (ii) his current students and postdoctorals: H. Niimi, K. Koh, B. Hinds, and B. Claflin. A research collaboration with the group of Professor H. Kurz at RWTH-Aachen, Germany, particularly G. Lüpke and C. Meyer in studying optical SHG at Si–SiO_2 interfaces is gratefully acknowledged.

[1] N. S. Saks, D. I. Ma, and W. B. Fowler, Appl. Phys. Lett. **67**, 374 (1995).
[2] M. L. Green, D. Brasen, K. W. Evans-Lutterodt, L. C. Feldman, K. Krisch, W. Lennard, L. Manchanda, H.-T. Tang, and M.-T. Tang, Appl. Phys. Lett. **65**, 848 (1994).
[3] K. L. Han, D. Wristers, T. S. Chen, C. Lin, K. Chen, J. Fulford, and D. L. Kwong, 1995 SDDM PC **1–2**, 261 (1995).
[4] D. R. Lee, G. Lucovsky, M. R. Denker, and C. Magee, J. Vac. Sci. Technol. A **13**, 607 (1995).
[5] D. R. Lee, C. Parker, J. R. Hauser, and G. Lucovsky, J. Vac. Sci. Technol. B **13**, 1778 (1995).
[6] G. Lucovsky, A. Banerjee, B. Hinds, B. Claflin, K. Koh, and H. Yang, J. Vac. Sci. Technol. B **15** (in press).
[7] K. Koh (unpublished); J. T. Fitch, Ph.D. thesis, NC State University.
[8] C. H. Bjorkman, C. E. Shearon, Jr., Y. Ma, T. Yasuda, G. Lucovsky, U. Emmerichs, C. Meyer, K. Leo, and H. Kurz, J. Vac. Sci. Technol. A **11**, 964 (1993).
[9] U. Emmerichs, C. Meyer, H. J. Bakker, F. Wolter, H. Kurz, G. Lucovsky, C. Bjorkman, T. Yasuda, Y. Ma, Z. Jing, and J. L. Whitten, J. Vac. Sci. Technol. B **12**, 2484 (1994).
[10] C. Meyer, G. Lüpke, U. Emmerichs, F. Wolter, H. Kurz, C. H. Bjorkman, and G. Lucovsky, Phys. Rev. Lett. **74**, 3001 (1995).
[11] T. Yasuda, Y. Ma, S. Habermehl, and G. Lucovsky, Appl. Phys. Lett. **60**, 434 (1992).
[12] G. Lucovsky *et al.*, *The Physics and Chemistry of* SiO_2 *and the* Si–SiO_2 *Interface*, edited by H. Z. Massoud, E. H. Poindexter, and C. R. Helms (Electrochemical Society, Pennington, 1996), p. 441.
[13] D. V. Tsu, G. N. Parsons, G. Lucovsky, and M. W. Watkins, J. Vac. Sci. Technol. A **7**, 1115 (1989).
[14] F. A. Cotton and G. Wilkinson, *Advanced Inorganic Chemistry*, 3rd ed. (Interscience, New York, 1972).
[15] J. T. Fitch, C. H. Bjorkman, G. Lucovsky, F. H. Pollak, and X. Yin, J. Vac. Sci. Technol. B **7**, 775 (1989).
[16] E. A. Irene (private communication).
[17] Z. Jing, G. Lucovsky, and J. L. Whitten, J. Vac. Sci. Technol. B **13**, 1613 (1995).
[18] G. Lucovsky, Z. Jing, and D. R. Lee, J. Vac. Sci. Technol. B **14**, 2832 (1996).
[19] T.-S. Tao, J. E. Rowe, H. Niimi, H. Yang, T. E. Madey, and G. Lucovsky (unpublished).
[20] X. Chen and J. M. Gibson, Appl. Phys. Lett. (in press).
[21] F. M. Ross, J. M. Gibson, and R. D. Twesten, Surf. Sci. **310**, 243 (1994).
[22] P. O. Hahn and M. Henzler, J. Vac. Sci. Technol. A **2**, 574 (1984).
[23] J. Didap *et al.*, in Ref. 12, p. 406.
[24] T. Sakoda *et al.*, *Proceedings of ISCSI*, Karuizawa, Japan (1996).